Biomed Microdevices (2012) 14:873–883
DOI 10.1007/s10544-012-9667-2

Microfabrication of cylindrical microfluidic channel networks for microvascular research

Zhouchun Huang · Xiang Li · Manuela Martins-Green · Yuxin Liu

Published online: 24 June 2012

Abstract Current methods for formation of microvascular channel scaffolds are limited with non-circular channel cross-sections, complicated fabrication, and less flexibility in microchannel network design. To address current limitations in the creation of engineered microvascular channels with complex three-dimensional (3-D) geometries in the shape of microvessels, we have developed a reproducible, cost-effective, and flexible micromanufacturing process combined with photolithographic reflowable photoresist and soft lithography techniques to fabricate cylindrical microchannel and networks. A positive reflowable photoresist AZ P4620 was used to fabricate a master microchannel mold with semi-circular cross-sections. By the alignment and bonding of two polydimethylsiloxane (PDMS) microchannels replicated from the master mold together, a cylindrical microchannel or microchannel network was created. Further examination of the channel dimensions and surface profiles at different branching levels showed that the shape of the microfluidic channel was well approximated by a semi-circular surface, and a multi-level, multi-depth channel network was created. In addition, a computational fluidic dynamics (CFD) model was used to simulate shear flows and corresponding pressure distributions inside of the microchannel and channel network based on the dimensions of the fabricated channels. The fabricated multi-depth cylindrical microchannel network can provide platforms for the investigation of microvascular cells growing inside of cylindrical channels under shear flows and lumen pressures, and work as scaffolds for the investigation of morphogenesis and tubulogenesis.

Keywords Reflow photoresist · PDMS · Multi-level · Multi-depth · Microchannels

1 Introduction

The creation of engineered microvascular channels with complex three-dimensional (3-D) geometries in the shape of microvessels presents a major challenge to the field of microvascular research and tissue engineering. There have been reports for making microvascular channels using conventional lithography methods (Emerson et al. 2006; Lu et al. 2004; Shevkoplyas et al. 2003; Kaihara et al. 2000), but all of such devices had employed rectangular, square or trapezoidal cross-sections of channels. Such channels impose widely varying fluid shear stresses and non-physiological geometries on cells in different channel positions (Zeng et al. 2006) that can induce significant variations in cell physiology (Fisher et al. 2001; Nerem et al. 1998). It is well accepted that the degree of shear stress imposed on luminal endothelial cells, which depends strongly on the geometry of the flow channel (Camp et al. 2008; Fisher et al. 2001; Nerem et al. 1998), affects their differentiation state (Riha et al. 2005), alignment and elongation (Kadohama et al. 2006), tight-junction formation (Colgan et al. 2007), gene expression (Warabi et al. 2004; McCann et al. 2005), and response to inflammatory stimuli (Surapisitchat et al. 2001; World et al. 2006). For these reasons, the geometry of the channel should replicate as closely as possible to the

Zhouchun Huang and Xiang Li contributed equally.

Z. Huang · X. Li · Y. Liu (✉)
Lane Department of Computer Science and Electrical Engineering,
West Virginia University,
Morgantown, WV 26506, USA
e-mail: yuxin.liu@mail.wvu.edu

M. Martins-Green
Department of Cell Biology and Neuroscience,
University of California at Riverside,
Riverside, CA 92521, USA

geometry of *in vivo* microvessels because of its essential role in the formation and maturation of vessels.

Microfabrication techniques can precisely control the fabricated structure's dimensions down to the micro-scale. They have been investigated for the fabrication of microchannels to closely approximate the geometry of *in vivo* microvessels, which adopt a roughly circular cross-section with radii between 30 and 300 μm (Young and Heath 2000). Typical substrates for fabricating microchannels are silicon (Liu et al. 2000; Agarwal et al. 2008; de Boer et al. 2000), glass (Rodriguez et al. 2003), and polymers (Borenstein et al. 2010). The efforts to create relatively well controlled circular cross-section of channels were reported by wet chemical etching (Seo et al. 2004), reactive gases such as SF_6, CF_4 and XeF_2 (Camp et al. 2008), ionized gas dry etching (Chen et al. 2011), femtosecond laser writing followed by chemical etching (Maselli et al. 2006; Crespi et al. 2010), electroplating combined with hot embossing and thermal bonding (Koskela 2010), thin film coating to modify the channel geometries (Borenstein et al. 2010), and embedded sacrificial elements (Bellan et al. 2009; Song et al. 2010). However, these fabrication methods involved toxic gases, limited with a maximum channel length (Abgrall and Gue 2007), and lacked the flexibilities for complicated channel designs. The fabricated channels were sometimes not suitable for long-term cell growing and co-culturing. These shortcomings limit their applications used for microvascular cells and research.

Since the inception of soft lithography (Xia and Whiteside 1998; Duffy et al. 1998), polydimethylsiloxane (PDMS) based microfluidic channels have been widely used for biological and chemical applications. The fabrications of circular cross-section of microchannels in PDMS were demonstrated by various molding techniques, which either directly molded the circular channels inside of PDMS or by PDMS replications from rounded master molds. Metal wires (Song et al. 2010), stainless steel needles (Chrobak et al. 2006), liquid PDMS remodified channels (Fiddes et al. 2010), and pressurized air streams (Abdelgawad et al. 2011) have been reported to directly create a single straight cylindrical channel in PDMS. These methods have limitations for fabricating channel networks, well controlled channel dimensions, and the geometries of the fabricated channels could vary from experiment to experiment. The fabrications of rounded master molds were demonstrated by photoresist melting (Chen et al. 2010; Wang et al. 2007), isotropic wet etching of the substrate molds (Shao et al. 2009), and mechanical micromilling (Wilson et al. 2011). These methods provide the flexibility for the channel designs, and the fabricated molds can be re-used for PDMS replications. However, the reported photoresist melting method resulted a flyer bow shaped cross-section, which caused the concern that the endothelial cells' seeding and growing in certain areas of the molded microchannels might be difficult to line into a monolayer. Mechanical micromilling is concerned with relatively larger variations and surface roughness in the small scales. In addition, the heights of the microfabricated channels are uniform throughout the whole pattern unless additional exposure and alignment steps are used. This limits microfabrication technologies for the creation of microchannel networks which obey Murray's law (Murray 1926a, b) to most approximately mimic the microvascular networks *in vivo*. Multi-level branching channels with multi-depths at different levels are preferred and need to be developed.

In this paper, we presented a convenient, cost-effective, and reproducible microfabrication approach to create both a single cylindrical microchannel and a circular cross-section of multi-depth microchannel network in PDMS by the combination of photolithographic photoresist reflow techniques and soft lithography. The geometries of the microchannels closely mimic the dimensions of microvessels *in vivo*.

2 Design and fabrication

2.1 Microchannel design

Conventional photolithography, in which light is projected through a patterned mask onto a photosensitive substrate, generally creates a rectangular or square cross-section of patterned features (Leong et al. 2010; Whitesides et al. 2001; Becker and Gartner 2008), which is not preferred for microvascular cell attachment as previously discussed. The photoresist reflow technique eliminates this limitation and is able to create a semi-circular cross-section of patterns. It involves melting photoresist structures to form curvature channels shaped by the surface tension of the liquid resist. However, the profiles of reflowed photoresist can be much more complex and dependent on certain parameters, such as polymeric nature of the photoresist, reflow temperature, resist boundary movement during reflowing, and outgassing (O'Neill and Sheridan 2002). PDMS replication using the reflow resist mold will create microchannels with semi-circular cross-sections. A circular cross-section of a channel can be created by aligning and bonding of two identical PDMS molds together.

As shown in Fig. 1, a single straight microchannel and a microchannel network were designed to mimic the actual sizes of microvessels *in vivo*. We designed the single channel with different diameters of 25 μm, 50 μm, 100 μm, 150 μm, and 200 μm (Fig. 1(a)). The design of a multiple branch channel network is based on Murray's law (Murray 1926a, b), which states that the cube of the radius of a parent branch equals the sum of the cubes of the radii of the

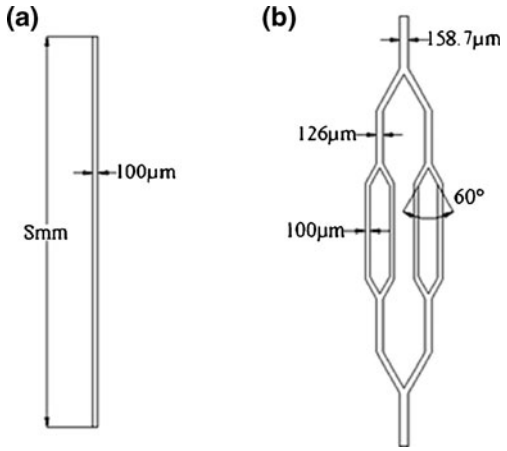

Fig. 1 Schematic designs of a single microchannel and a microchannel network. (**a**) A straight channel (width: 100 μm and length: 8 mm as an example). (**b**) A network with multi-branch channels. As an example, the channel widths at different branch channels were calculated based on the Murray's law

daughters (Sherman 1981). Figure 1(b) shows an example of the network design with the smallest channel diameter set as 100 μm, and the diameters of its upper branch channels were calculated based on Murray's law. The angles at the bifurcations were designed as 60 ° to mimic the histological conditions so that the channel network design matched the microvascular vessel network *in vivo* for maintaining the fluid flow at a required level (Murray 1926a, b; Zamir and Medeiros 1982; Gafiychuk and Lubashevsky 2001).

2.2 Computational fluidic dynamics simulation

The luminal surface of the blood vessel and its endothelial surface are constantly exposed to hemodynamic shear stress (Davies 1995; Fung 1997). For microvessel morphogenesis, shear flows and associated lumen pressures are critical parameters that affect vessel maturation and structure, barrier functions and permeability, and regulation of key enzymes (Meeson et al. 1996; Van Royen et al. 2001; Schaper 2001; Tarbell 2010; Potter et al. 2011). The magnitude of the shear stress can be estimated in most of the vasculature by Poiseuille's law $\left(\tau_s = \frac{4\mu Q}{\pi R^3}\right)$, in which τ_s is the hemodynamic shear stress, μ is the blood viscosity, Q is the flow rate, and R is the radius of the vessel. Poiseuille's law states that shear stress is proportional to blood flow viscosity, and inversely proportional to the third power of the internal radius (Kamiya et al. 1984; LaBarbera 1990). Measurements using different modalities show that shear stress ranges from 1 to 6 dyne/cm^2 (0.1 to 0.6 pascals (Pa)) in the venous system and between 10 and 70 dyne/cm^2 (1 to 7 Pa) in the arterial vascular network (Malek et al. 1999). To analyze the variations of the fluid flows and pressure distributions inside of the designed microchannels and networks, a fluid dynamic analysis using COMSOL multiphysics software (Version 4.0.0.982, COMSOL Inc. USA) was performed to numerically simulate fluid flows and shear stress distributions. It will provide guidance for our future research with the microvascular cells seeding and growing inside of these channels to satisfy *in vivo* hemodynamic conditions under fluid flow and pressure conditions.

The fluid dynamics analysis considers the solution of the 2D Navier–Stokes equations in a stationary case. The procedures to implement the COMSOL analysis were: Select space dimension; Add and set the model as laminar flow and stationary; Define length unit as micrometer; Import the pattern file from AutoCAD (Autodesk, Inc. USA); Define the fluid properties; Define the appropriate boundary conditions (the combinations between inflow conditions (pressure, velocity, or flow rate) and outflow conditions (pressure, velocity, or flow rate), and no-slip wall); Create mesh; Under the Study menu, select PARallel sparse DIrect linear SOlver (PARDISO) and execute the calculation. PARDISO, an embedded solver in COMSOL, is used to solve the partial differential equation (PDE) system governed by the Navier–Stokes equations for a Newtonian and incompressible fluid (Stalder et al. 2011).

The meshing was realized using the free triangular function that automatically created an unstructured triangular mesh of the subdomain. Free triangular function has the flexibility to automatically control the number, size, and distribution of elements based on the available computing capability of the working computer. The total subdomain elements used in the simulation were set as 108,450 with the maximum element size of 8 μm. In order to reliably assess shear stresses at the certain boundary regions of interest, such as curvatures along the network, resolution of curvature was adjusted to give a finer mesh along curved boundaries.

Human blood was taken as a reference fluid during the simulation and the fluid properties were defined with a constant density (1060 kg/m^3) and a constant dynamic viscosity μ (0.005 N•s/m^2) (Gnasso et al. 1996). The appropriate boundary conditions were defined based on the flow shear stresses experienced by the endothelial surface in similarly sized microvessels *in vivo* (Malek et al. 1999). For example, we set the inflow and the outflow pressure difference as 540 Pa by defining the inflow pressure as 540 Pa and the outflow pressure as 0 Pa, and defined no-slip wall conditions along the internal surface of microchannel network. As shown in Fig. 2, the corresponding flow velocity and shear stress distributions were shown in Fig. 2(a), (b) and (c), respectively. Using the simulation model, we are able to estimate the flow rates (i.e. 1.8~4.7 μL/min) and corresponding shear stresses (i.e. 1.05~2 Pa) along the channel network based on the channel dimensions and given pressure difference.

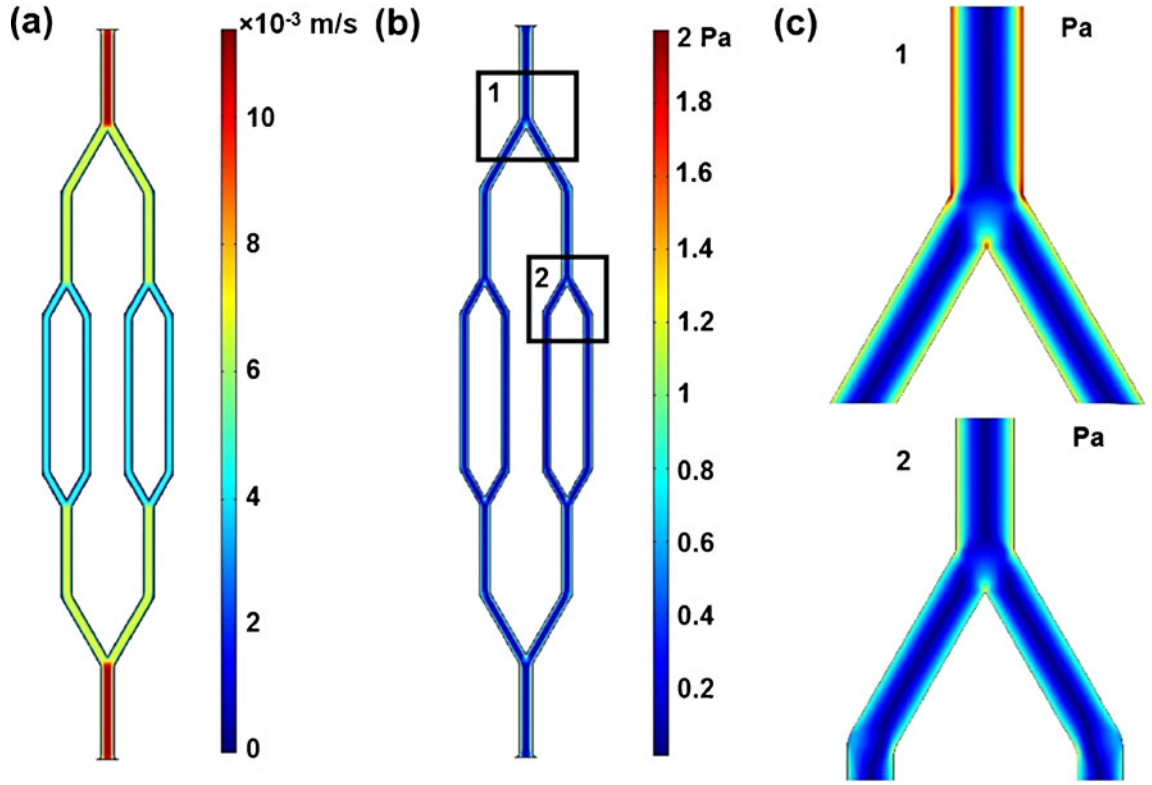

Fig. 2 COMSOL simulation model for the microchannel network. (**a**) Flow velocity field (m/s); (**b**) Shear stress distribution (Pa); (**c**) Shear stress distributions at different regions of the network. c-1 is for the region of b-1 and c-2 is for the region of b-2

In COMSOL simulation, the shear stresses were obtained based on $\tau = \gamma \cdot \mu$, where τ (Pa) is the wall shear stress, γ $(1/s)$ is local shear rate, and μ is the dynamic viscosity (N•s/m^2) (Couzon et al. 2009), which is the modified equation of Poiseuille's law. Additionally, variations of the inflow and outflow boundary conditions, such as increasing or decreasing the inflow/outflow pressures or inflow/outflow velocities within the physiological range, can increase or decrease the scale of the wall shear stresses to match the *in vivo* situations, but the actual shear pattern remained nearly unchanged within the network.

2.3 Fabrication of master molds with semi-circular cross-section

The positive reflow photoresist AZ P4620 (AZ Electronic Materials) works well for patterning features down to 5 μm, and the film thickness can reach up to 60 μm with different spin-coating protocols, which makes it suitable as a mold material for the fabrication of the microvascular channels which require different diameters or aspect ratios. In our fabrication procedures, conventional photolithography followed by resist reflowing was applied for the master mold fabrication (Fig. 3). Both the single channel and the network patterns were designed as discussed in the above section, drawn by AutoCAD, and transferred into a photomask.

Silicon wafers were pre-cleaned and hard baked at 150 °C for 1 h to enhance the adhesion between the wafers and the AZ P4620 (Fig. 3(a)). The thickness of the spun AZ P4620 is limited to 30 μm. For a microchannel with a larger diameter, we used a double-coating procedure to get a thicker AZ 4620 film. The first layer of AZ P4620 (10~30 μm) was spun onto the substrate and baked at 110 °C for 90 secs, and then, the second layer of AZ P4620 (10~30 μm) was spun on top of the first layer and baked at 110 °C for 3 mins (Fig. 3(b)). The photoresist film was UV exposed using a flood exposure system (OAI model 150) and followed by the development in AZ 400 K developer diluted with deionized (DI) water (1:2 (v/v)) for 4 mins (Fig. 3(c) and (d)). Finally, the patterned AZ P4620 was reflowed and rounded at 120 °C for 4 mins to form a half-cylindrical channel with a semi-circular cross-section (Fig. 3(e)), which was used as a master mold for PDMS replication.

2.4 PDMS scaffold fabrication

PDMS solutions were prepared at the ratio of 10:1 (base: curing agent) and cast onto the AZ P4620 master mold

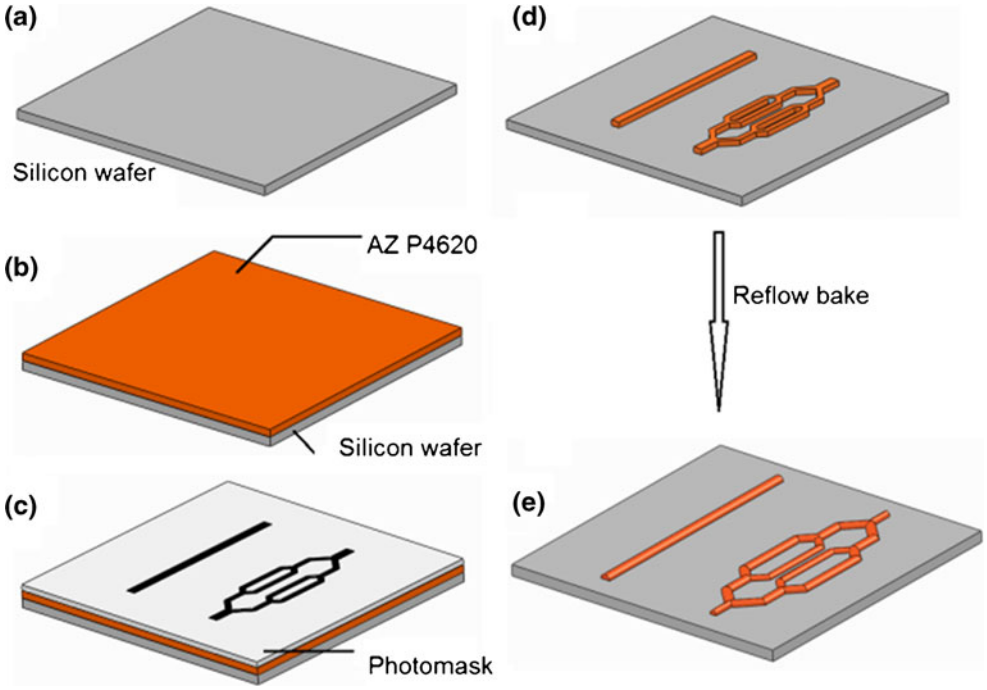

Fig. 3 The schematic fabrication procedures for AZ P4620 master molds. (**a**) A pre-cleaned silicon substrate; (**b**) Two layers of positive photoresist AZ P4620 were spun onto the silicon substrate, respectively. The second layer of AZ P4620 was applied after the first layer was baked and dried; (**c**) The photoresist was exposed under the UV light through the mask; (**d**) The patterned structure after AZ 400 K development; (**e**) The reflow photoresist patterns with semi-circular cross-sections after the reflow at 120 °C for 4 mins

twice, respectively (Fig. 4(a) and (b)). The PDMS layers together with the master molds were baked at 60 °C for 3 hrs to cure the PDMS, and then, the PDMS layers were peeled off the molds and treated with 30 secs oxygen plasma (Fig. 4(c)). They were aligned under an optical microscope and bonded together, which formed a microchannel with a circular cross-section (Fig. 4(d)).

3 Results and discussions

3.1 AZ P4620 master mold

Figure 5(a) and (b) show scanning electron microscope (SEM, JEOL JSM-7600 F) images of the AZ P4620 photoresist mold before and after the reflow process, respectively. Figure 5(c) and (d) show the replicated PDMS channels from the molds before and after reflow, respectively. The cross-section of the PDMS microchannel indicates the profile changes from a rectangular to a semi-circular cross-section. The reflow process involves the melting of the patterned photoresist, and the liquid resist surfaces are pulled into a shape which minimizes the energy of the system (Daly et al. 1990; Schilling et al. 2000). A cooling and solidification phase is followed the melting process. In ideal conditions, the shape of the reflowed photoresist will be well approximated by a semi-circular surface. However, several parameters are involved and make the profiles more complex, such as critical angle at which the photoresist meets the solid substrate, material evaporation, temperature gradient, outgassing, resist boundary movement, variation of substrate, and polymeric nature of resists. For example, the magnitude of the critical angle is governed by the surface tension of the liquid resist, the surrounding air, and the substrate properties (de Gennes 1985). In addition, the

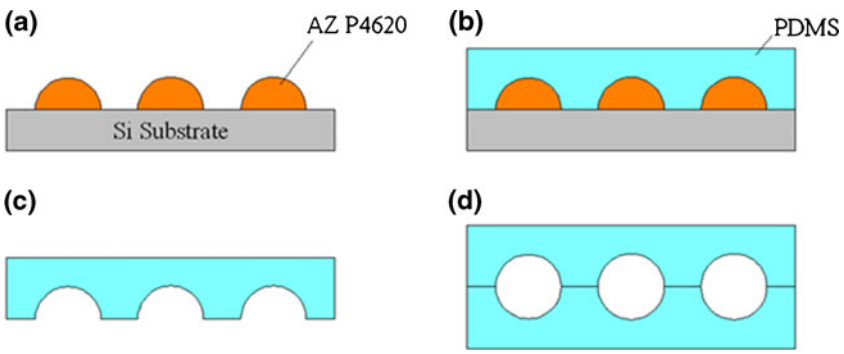

Fig. 4 The schematic fabrication procedures for cylindrical microchannels in PDMS. (**a**) The reflow AZ P4620 microchannel network; (**b**) Cast PDMS solution onto the AZ P4620 mold; (**c**) The cured PDMS layer; (**d**) Aligned and bonded two PDMS layers to form microchannels with circular cross-sections

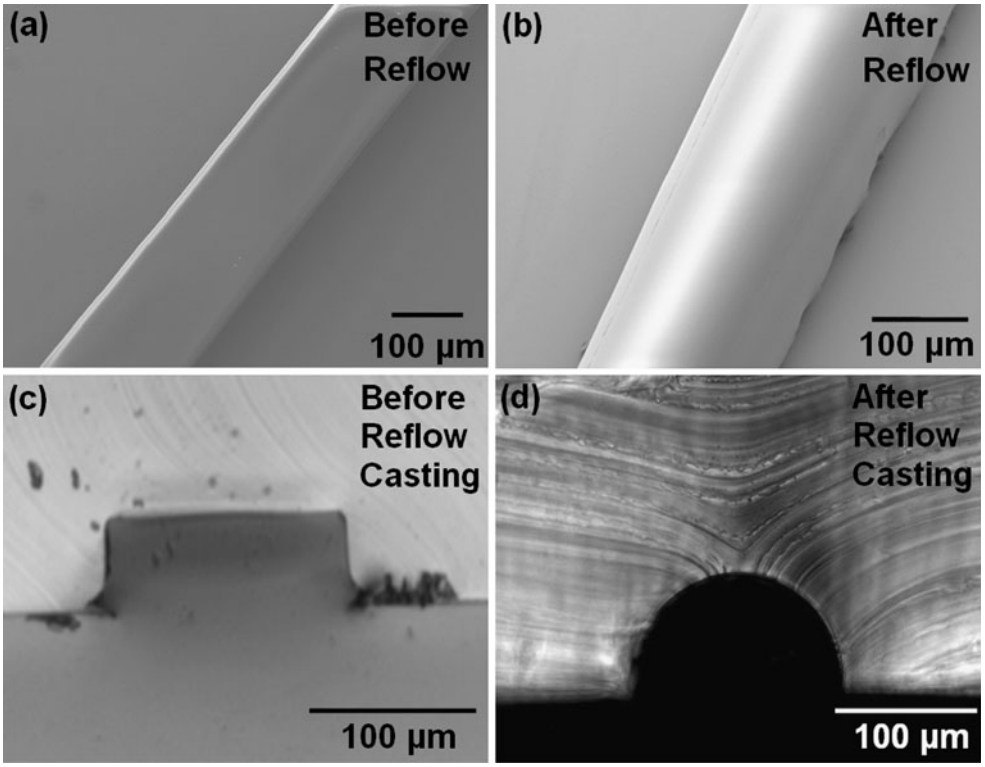

Fig. 5 SEM shows the developed AZ P4620 photoresist (**a**) before reflow; (**b**) after reflow; (**c**) molded PDMS showed the cross section of the resist before reflowing; the picture shows a rectangular cross section; (**d**) molded PDMS showed a semi-circular cross-section of the resist after reflowing; The cross section after reflow was controlled by the initial dimension design of the pattern and reflow temperature

temperature and timing during the reflow process can result in a volume change causing the boundary to move and hence varying the critical angle (Elias 1997). Therefore, variations in this critical angle, resulting in different rounding profiles of the reflow resist, will occur if the reflow temperature and timing are varied, the substrate is non-uniform, or the liquid/substrate interface moves (Sekimoto et al. 1987; Voinov 1999). To get a cylindrical surface for a given width of microchannel, one particular volume of the resist is required. If cylindrical surfaces with different radii are required through a microchannel network, it is necessary to vary the width of the microchannels, resulting in variations in the volumes, at different regions in the network. Deviations from the cylindrical surface could occur when the volume used to produce the microchannel varies from the volume necessary to produce the cylindrical case (Daly et al. 1990). In addition, an ideal volume for getting a cylindrical surface must make allowance for the effect of material evaporation during the reflow process (Jay and Stern 1994). To successfully fabricate a single cylindrical channel or a cylindrical channel network with different radii, the resists widths/volumes, reflow temperatures and timing, critical angles, boundary movement, and resist and substrate properties must be considered.

More details have been investigated and discussed in other published results (Schilling et al. 2000; O'Neill and Sheridan 2002). The film thickness required for an ideal cylindrical case can be pre-determined given a required width and focal length of the microchannel as $H = \frac{1}{2E}\left[\frac{R^2}{r}\sin^{-1}\left(\frac{r}{R}\right) - R + h\right]$, where H is the required spun-film thickness, r is half of the channel width, R is the constant radius of curvature, h is the central height of the curvature, and E is the ratio of resist volumes of the microchannel before and after reflowing (O'Neill and Sheridan 2002). These previous findings provide us with references for design and fabrication of semi-circular microchannels in this research work.

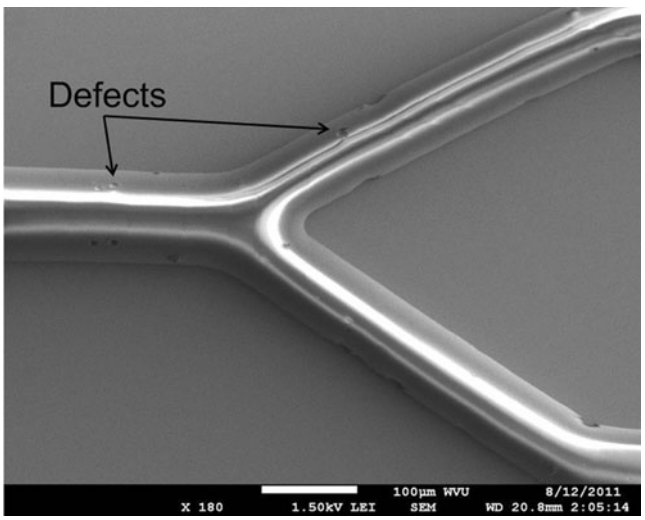

Fig. 6 SEM shows small defects on the reflowed mold

Additionally, during the fabrication process, it was noticed that small hole defects appeared on the photoresist surface when the reflow baking temperatures were higher than 120 °C or longer baking (more than 4 mins) was performed (Fig. 6). It was concluded that these small defects could be possibly caused by outgassing, which can affect the channel profile formation in causing gas bubbles in the resist during reflow baking. The outgassing can be solved by lowering the baking temperatures.

The geometries of *in vivo* microvessels adopt a roughly circular cross-section with radii between 30 and 300 μm, thus the fabricated microchannels are required to closely

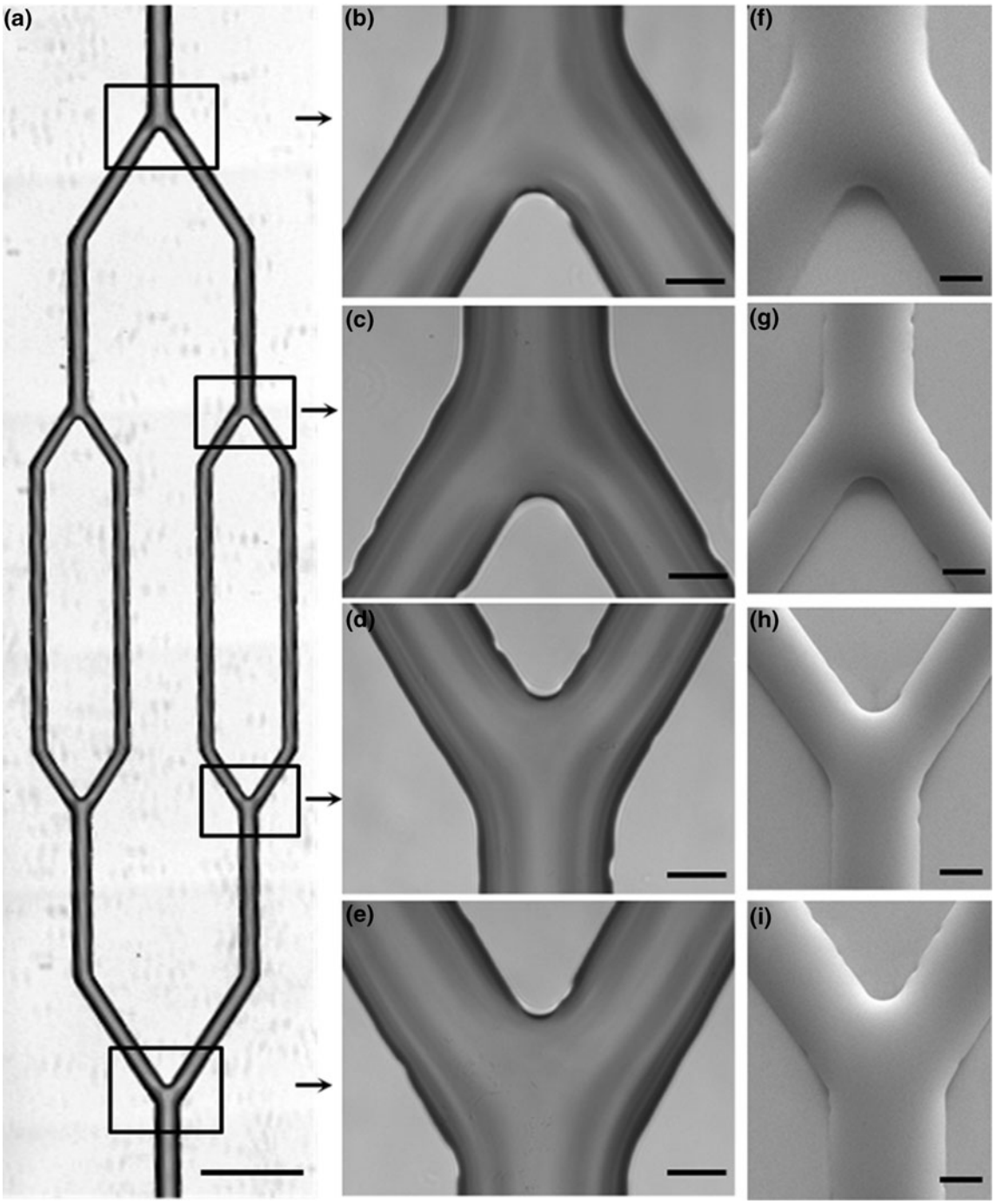

Fig. 7 Microscope images show the smooth surface transitions at bifurcations. (**a**) A PDMS channel network. The frames indicate the bifurcations through the channel network and the arrows indicate the panels at the right side. The scale bar is 500 μm. (**b**–**e**) Optical images show the smooth surface transitions on the PDMS channel network. The scale bar is 50 μm. (**f**–**i**) SEM images show the smooth surface transitions on the AZ P4620 resist mold. The scale bar is 50 μm

approximate these geometries. According to AZ® P4000 Thick Film Photoresist Datasheet from AZ Electronic Materials, a 20–30 μm thick AZ P4620 film (before reflow) can be easily obtained by adjusting the coating speeds in the range lower than 1000 rpm. To get thicker films, we used a double coating procedure, which can achieve the film thicknesses up to 60 μm before reflow. For a film thickness above 60 μm, additional coating procedure can be used. However, it may result in a non-uniform film thickness and would be difficult to determine accurate exposure doses. Other high viscous reflow photoresist, such as AZ P4903, AZ 9260, and AZ 40 XT, would be recommended for getting a thicker film or pattern. For example, using AZ 40 XT has been demonstrated to fabricate posts of 80 μm in height at different temperatures (varying from 110 °C to 130 °C) and for different time (varying from 30 secs to 4 mins) (Application notes from MicroChemicals). It would be more convenient to fabricate even thicker films or pattern by a double coating procedure. Three of resists mentioned above are positive reflow resists, of which one will be chosen based on different applications for cylindrical microchannels or micropatterns. The fabrication protocols of using different reflow resists will be determined and varied by resist viscosities, spin coatings, substrate materials, optical exposures, and reflow temperatures and time. Furthermore, the properties of the resist may also vary slightly with changes in storage temperature and humidity (O'Neill and Sheridan 2002).

Furthermore, we examined the AZ P4620 master mold (after reflow) and PDMS channels cast from the reflowed resist molds using SEM and optical microscope, respectively (Fig. 7). The bifurcations were particularly examined through the channel network. As shown in the figures, the surfaces were smooth at the transitions from a larger channel to two smaller channels both in the resist mold and in the PDMS mold. Additionally, local resist melting was observed along the edges of the channels because of resist-substrate adhesion and boundary movement.

3.2 PDMS cylindrical microchannels

Two identical PDMS layers were cast from the same resist mold, each of which contains either a microchannel or a channel network with semi-circular cross-sections (Fig. 5 (d)). They were aligned and bonded together under the microscope to form a permanent sealing between two layers after oxygen plasma treatment. Figure 8(a) and (b) show the circular cross-section of a microchannel and a channel network with two microchannels, respectively.

3.3 Microchannel dimensions

To determine the dimension variations between the designed patterns and actual fabricated channels, we compared the results of measured channel diameters before the reflow, after the reflow, and after PDMS soft lithography. To prevent the variations caused by additional fabrication factors, we kept the same PDMS mixing ratios, baking temperature, and baking duration. However, because the fabrication of different diameters of semi-circular patterns requires different photoresist film thicknesses and exposure doses, we found that channel widths were reduced (6–10 %) during the processes involved with photolithography and development as shown in table 1. Additionally, the reflow process also decreased the channel widths by 2 % on average because of photoresist volume reductions and boundary movement (Elias 1997; O'Neill and Sheridan 2002). PDMS microchannel normally shrinks while curing and this shrinkage is dependent upon curing temperature, the ratio of base to curing agent, and curing time. From our results, both PDMS microchannel shrinkage and swelling occurred, and the ratio of the changes were small compared with the changes caused in the photolithographic processes. Based on the discussion above, the shrinkage of microchannels mainly occurred before the reflow. Each master mold should be designed to compensate for this shrinkage, and the fabrication parameters need to be optimized to have the fabricated channel dimensions more accurately closer to the designed dimensions.

To most approximately mimic the microvascular networks *in vivo* based on Murray's law, multi-level branching channels with multi-depths at different levels are required. A direct-write method for the creation of multi-depth microfluidic channels previously reported for the potential benefits of resembling *in vivo* physiological vascular conditions in a biomimetic design (Lim et al. 2003). Multi-depth channel network can lower the overall resistance and keep more

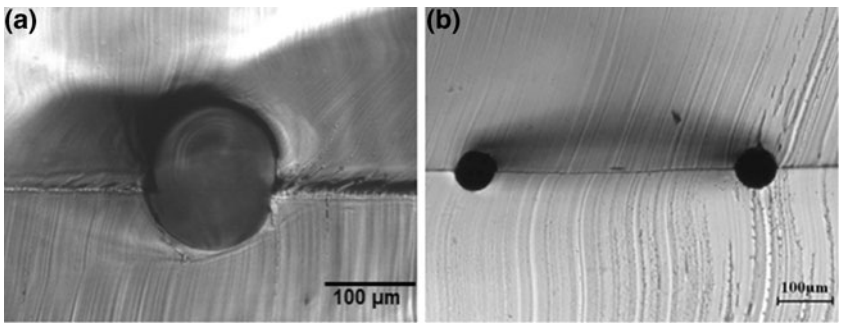

Fig. 8 Cylindrical microfluidic channels formed in PDMS. (**a**) A cylindrical microchannel with a circular cross-section; (**b**) The circular cross-section of a microchannel network shows two channels

Table 1 Cross-sectional dimensions (unit: μm)

Designed diameters	Channel width before reflow	Diameters after reflow	Diameters in PDMS
25	23.26	23.17	24
50	46.92	44.67	46
100	88.95	85.48	85
150	138.96	137.01	136
200	180.55	180.55	179

uniform flow velocities throughout the network than the uniformly thickness channel generated by the planar patterning techniques. With this consideration, we examined the cross-sections of the molded PDMS channels at the different branching levels in the network. The channel widths and central heights were measured using NIS-Elements imaging software (Nikon). For example, as shown in the Fig. 9, the widths of channels at different branching levels are 65 μm, 78 μm, and 92 μm. The corresponding central heights are 34 μm, 37 μm, and 45 μm, respectively. There might be some variations in these measurements because of the way that PDMS channels were cut. At each branching level, the central height of the channel is very close to the half width of the channel, which indicated that the shape of the reflowed photoresist can be well approximated by a semi-circular surface under well controlled conditions. As

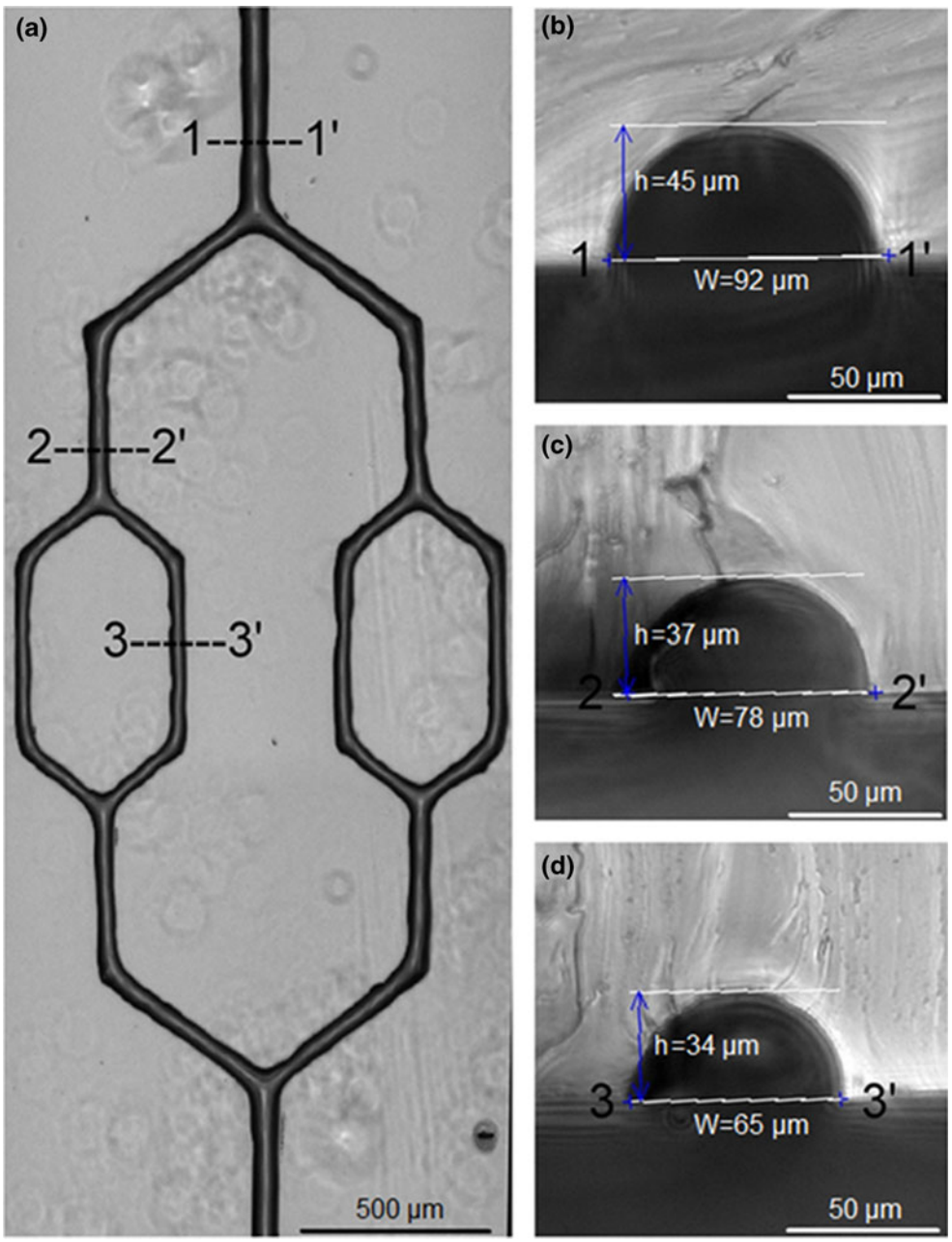

Fig. 9 (**a**) Reflowed AZ P4620 channel network mold; 1-1', 2-2' and 3-3' indicated each branching channel, respectively. (**b**–**d**) Cross-sections of PDMS molds show channel dimensions at each level (1-1', 2-2', and 3-3'), respectively. The width and height of each channel were shown as in the figures

discussed in the AZ P4620 master mold section, the reflowed channel surface profiles are determined by the design channel widths, the volume of the photoresist patterns, and reflowing process. Our results show that the photoresist reflow technique can create multi-depth branching channel networks in a more convenient approach by photoresist reflow techniques, and allow for the design of microvascular biomimetic systems which obey Murray's Law.

4 Conclusions

In conclusion, a flexible, cost-effective, and reproducible micromanufacturing method, combining with photolithographic reflow photoresist and PDMS soft lithography, was developed for fabricating cylindrical microchannels and microchannel networks with circular cross-sections. The designs of a microchannel and microchannel networks were based on Murray's Law to mimic the geometry of microvascular microvessels *in vivo*. A COMSOL simulation model was developed to analyze fluid flows and lumen pressure distributions inside of the microchannels. Several fabrication parameters, such as reflow parameters and shrinkage, were discussed, and it was indicated that compensation is required for microchannel design to closely approximate microvessels. The multi-depth microfluidic channel network would allow for the flow patterns that are more physiological relevant to *in vivo* conditions and are expected to benefit microvascular research. For example, the fabricated cylindrical microchannels and networks can either work as a scaffold for investigating microvascular cells seeding and growing inside of cylindrical channels under shear flows and lumen pressures or as a mold for further fabrication of tissue scaffolds for morphogenesis and tubulogenesis.

Acknowledgments Xiang Li and Zhouchun Huang are co-first authors. We thank Mr. Michael Martin for proofreading and editing the paper. This research work was supported by WVU EPSCoR program funded by the National Science Foundation (EPS-1003907). Partial support for this work was provided by the National Science Foundation's ADVANCE IT Program under Award HRD-1007978. Any opinions, findings, and conclusions or recommendations expressed in this material are those of the author(s) and do not necessarily reflect the views of the National Science Foundation. The microfabrication work was done in WVU Shared Research Facilities (Cleanroom facilities) and Microfluidic Integrative Cellular Research on Chip Laboratory (MICRoChip Lab) at West Virginia University.

References

M. Abdelgawad, C. Wu, W.-Y. Chien, W.R. Geddie, M.A.S. Jewett, Y. Sun, Lab Chip **11**, 545 (2011)
P. Abgrall, A.M. Gue, J. Micromech. Microeng. **R15**, 17 (2007)
A. Agarwal, N. Ranganathan, W.L. Ong, K.C. Tang, L. Yobas, Sens. Actuators **A 142**, 80 (2008)
Application notes from MicroChemicals: Reflow of Photoresist, http://www.microchemicals.eu/technical_information
H. Becker, C. Gartner, Anal. Bioanal. Chem. **390**, 89 (2008)
L.M. Bellan, S.P. Singh, P.W. Henderson, T.J. Porri, H.G. Craighead, J.A. Spector, Soft Matter **5**, 1354 (2009)
J.T. Borenstein, M.M. Tupper, P.J. Mack, E.J. Weinberg, A.S. Khalil, J. Hsiao, G. García-Cardeña, Biomed. Microdevices **12**, 71 (2010)
J.P. Camp, T. Stokol, M.L. Shuler, Biomed. Microdevices **10**, 179 (2008)
Y.-C. Chen, G.-Y. Chen, Y.-C. Lin, G.-J. Wang, Microfluid. Nanofluid. **9**, 585 (2010)
J.A. Chen, Y. Zheng, Q. Tan, Y.L. Zhang, J. Li, W.R. Geddie, M.A.S. Jewett, Y. Sun, Biomicrofluidics **5**, 014113 (2011)
K.M. Chrobak, D.R. Potter, J. Tien, Microvasc. Res. **71**, 185–196 (2006)
O.C. Colgan, G. Ferguson, N.T. Collins, R.P. Murphy, G. Meade, P.A. Cahill, P.M. Cummins, Am. J. Physiol. Heart Circ. Physiol. **292**, H3190 (2007)
C. Couzon, A. Duperray, C. Verdier, Eur. Biophys. J. **38**, 1035 (2009)
A. Crespi, Y. Gu, B. Ngamson, H.J.W.M. Hoekstra, C. Dongre, M. Pollnau, R. Ramponi, H.H. van den Vlekkert, P. Watts, G. Cerullo, R. Osellame, Lab Chip **10**, 1167 (2010)
D. Daly, R.F. Stevens, M.C. Hutley, N. Davies, Meas. Sci. Technol. **1**, 759 (1990)
P.F. Davies, Physiol. Rev. **75**, 519–560 (1995)
M.J. de Boer, R.W. Tjerkstra, J.W. Berenschot, H.V. Jansen, G.J. Burger, J.G.E. Gardeniers, M. Elwenspoek, A. van den Berg, J. Microelectromech. Syst. **9**, 94 (2000)
de Gennes, Rev. Mod. Phys. **57**, 827–863 (1985)
D.C. Duffy, J.C. McDonald, O.J.A. Schueller, G.M. Whitesides, Anal. Chem. **70**, 4974 (1998)
H. G. Elias, VCH Publishers, New York (1997)
D.R. Emerson, K. Cieslicki, X. Gu, R.W. Barber, Lab Chip **6**, 447 (2006)
L.K. Fiddes, N. Raz, S. Srigunapalan, Biomaterials **31**, 3459 (2010)
A.B. Fisher, S. Chien, A.I. Barakat, R.M. Nerem, Am. J. Physiol. Lung Cell. Mol. Physiol. **281**(3), L529 (2001)
Y. C. Fung, New York, NY: Springer; (1997)
V.V. Gafiychuk, I.A. Lubashevsky, J. Theor. Biol. **212**, 1 (2001)
A. Gnasso, C. Carallo, C. Irace, V. Spagnuolo, G. De Novara, P.L. Mattioli, A. Pujia, Circulation **94**, 3257–3262 (1996)
T.R. Jay, M.B. Stern, Opt. Eng. **33**, 3552–3555 (1994)
T. Kadohama, N. Akasaka, K. Nishimura, Y. Hoshino, T. Sasajima, B.E. Sumpio, Endothelium **13**, 43 (2006)
S. Kaihara, J. Borenstein, R. Koka, S. Lalan, E.R. Ochoa, M. Ravens, H. Pien, B. Cunningham, J.P. Vacanti, Tissue Eng. **6**, 105 (2000)
A. Kamiya, R. Bukhari, T. Togawa, Bull. Math. Biol. **46**, 127–137 (1984)
J. Koskela, Master's thesis, Tampereen teknillinen yliopisto. (2010)
M. LaBarbera, Science **249**, 992–1000 (1990)
T.G. Leong, A.M. Zarafshar, D.H. Gracias, Small **6**, 792 (2010)
D. Lim, Y. Kamotani, B. Cho, J. Mazumder, S. Takayama, Lab Chip **3**, 318 (2003)
R.H. Liu, M.A. Stremler, K.V. Sharp, M.G. Olsen, J.G. Santiago, R.J. Adrian, H. Aref, D.J. Beebe, J. Microelectromech. Syst. **9**, 190 (2000)
H. Lu, L.Y. Koo, W.M. Wang, D.A. Lauffenburger, L.G. Griffith, K.F. Jensen, Anal. Chem. **76**, 5257 (2004)
A.M. Malek, S.L. Alper, S. Izumo, JAMA **282**(21), 2035–2042 (1999)
V. Maselli, R. Osellame, G. Cerullo, R. Ramponi, P. Laporta, L. Magagnin, P.L. Cavallotti, Appl. Phys. Lett. **88**, 191107 (2006)
J.A. McCann, S.D. Peterson, M.W. Plesniak, T.J. Webster, K.M. Haberstroh, Ann. Biomed. Eng. **33**, 328 (2005)
A. Meeson, M. Palmer, M. Calfon, R. Lang, Development **122**, 3929 (1996)
C.D. Murray, Proc Natl Acad Sci USA **12**, 207 (1926a)
C.D. Murray, J. Gen. Physiol. **9**, 835 (1926b)
R.M. Nerem, R.W. Alexander, D.C. Chappell, R.M. Medford, S.E. Varner, W.R. Taylor, Am. J. Med. Sci. **316**(3), 169 (1998)

F.T. O'Neill, J.T. Sheridan, Optik **113**, 391 (2002)
C.M. Potter, M.H. Lundberg, L.S. Harrington, C.M. Warboys, T.D. Warner, R.E. Berson, A.V. Moshkov, J. Gorelik, P.D. Weinberg, J.A. Mitchell, Arterioscler. Thromb. Vasc. Biol. **31**, 384 (2011)
G.M. Riha, P.H. Lin, A.B. Lumsden, Q. Yao, C. Chen, Ann. Biomed. Eng. **33**, 772 (2005)
I. Rodriguez, P. Spicar-Mihalic, C.L. Kuyper, G.S. Fiorini, D.T. Chiu, Anal. Chim. Acta **496**, 205 (2003)
W. Schaper, Circulation **104**, 1994 (2001)
A. Schilling, R. Merz, C. Ossmann, H.P. Herzig, Opt. Eng. **39**, 2171–2176 (2000)
K. Sekimoto, R. Oguma, K. Kawasaki, Ann. Phys. **176**, 359–392 (1987)
C.T. Seo, C.H. Bae, D.S. Eun, J.K. Shin, J.H. Lee, Jpn. J. Appl. Phys. **43**, 7773 (2004)
J. Shao, L. Wu, J. Wu, Y. Zheng, H. Zhao, Q. Jin, J. Zhao, Lab Chip **9**, 3118 (2009)
T.F. Sherman, J. Gen. Physiol. **78**, a 431 (1981)
S.S. Shevkoplyas, S.C. Gifford, T. Yoshida, M.W. Bitensky, Microvasc. Res. **65**, 132 (2003)
S.H. Song, C.K. Lee, T.J. Kim, I.C. Shin, S.C. Jun, H.I. Jung, Microfluid. Nanofluid. **9**, 533 (2010)
A.F. Stalder, Z. Liu, J. Hennig, J.G. Korvink, K.C. Li, and M. Markl, Part 1, 27-38, Springer Science (2011)
J. Surapisitchat, R.J. Hoefen, X. Pi, M. Yoshizumi, C. Yan, B.C. Berk, Proc. Natl. Acad. Sci. U. S. A. **98**, 6476 (2001)
J.M. Tarbell, Cardiovasc. Res. **87**, 320 (2010)
N. Van Royen, J.J. Piek, W. Schaper, C. Bode, I. Buschmann, J. Nucl. Cardiol. **8**, 687 (2001)
O.V. Voinov, Jour. Appl. Mech. Tech. Phys. **40**, 86–92 (1999)
G.-J. Wang, K.-H. Ho, S.-H. Hsu, K.-P. Wang, Biomed. Microdevices **9**, 657 (2007)
E. Warabi, Y. Wada, H. Kajiwara, M. Kobayashi, N. Koshiba, T. Hisada, M. Shibata, J. Ando, M. Tsuchiya, T. Kodama, N. Noguchi, Free Radic. Biol. Med. **37**, 682 (2004)
G.M. Whitesides, E. Ostuni, S. Takayama, X. Jiang, D.E. Ingber, Annu. Rev. Biomed. Eng. **3**, 335 (2001)
M.E. Wilson, N. Kota, Y.T. Kim, Y. Wang, D.B. Stolz, P.R. LeDuc, O.B. Ozdoganlar, Lab Chip **11**, 1550 (2011)
C.J. World, G. Garin, B. Berk, Curr. Atheroscler. Rep. **8**, 240 (2006)
Y. Xia, G.M. Whiteside, Annu. Rev. Mater. Sci. **28**, 153 (1998)
B. Young, J. W. Heath, Wheater's functional histology: A Text and Colour Atlas, 4th edn. (Churchill livingstone, 2000)
M. Zamir, J.A. Medeiros, J. Gen. Physiol. **79**, 353 (1982)
Y. Zeng, T.-S. Lee, P. Yu, P. Roy, H.-T. Low, J. Biomech. Eng. **128**, 185 (2006)